University of Bath

Alternative formats
If you require this document in an alternative format, please contact:
openaccess@bath.ac.uk

Towards Effective Energy Harvesting from Stacks of Soil Microbial Fuel Cells

Jakub Dziegielowski[1,2], Benjamin Metcalfe[2,3], Mirella Di Lorenzo[1,2]*

[1]*Department of Chemical Engineering, University of Bath, BA2 7AY, Bath, UK*

[2]*Centre for Biosensors, Bioelectronics and Biodevices, University of Bath, BA2 7AY, Bath, UK*

[3]*Department of Electronic and Electrical Engineering, University of Bath, BA2 7AY, Bath, UK*

* Corresponding Author: m.di.lorenzo@bath.ac.uk

Abstract

The 2050 net-zero carbon target can only be achieved with renewable energy solutions that can drastically reduce carbon emissions. Soil microbial fuel cells (SMFCs) have significant potential as a low-cost and carbon-neutral energy conversion technology. Finding the most practical and energy efficient strategy to operate SMFCs is crucial for transitioning this technology from the lab to field implementations. In this study, an innovative self-sustaining and model-based energy harvesting strategy was developed and tested for the first time on SMFC stacks. The model, based on a first-order equivalent electrical circuit (EEC), enables real-time and continuous maximum power point tracking, without the need for offline analysis of electrochemical parameters. Power extraction from the SMFCs to fully charge a 3.6 V NiMH battery, was carried out for 24 hours: the longest test duration reported so far on biological fuel cells for such energy harvesting strategy. A novel second-order EEC was also proposed to better describe the electrical dynamics of the SMFC. Our results provide important advances on both accurate model-based electrochemical parameter identification techniques and maximum power point tracking algorithms, for optimal energy extraction from SMFCs. Consequently, this study paves the way for successful implementations of SMFCs towards viable green energy solutions.

GRAPHICAL ABSTRACT
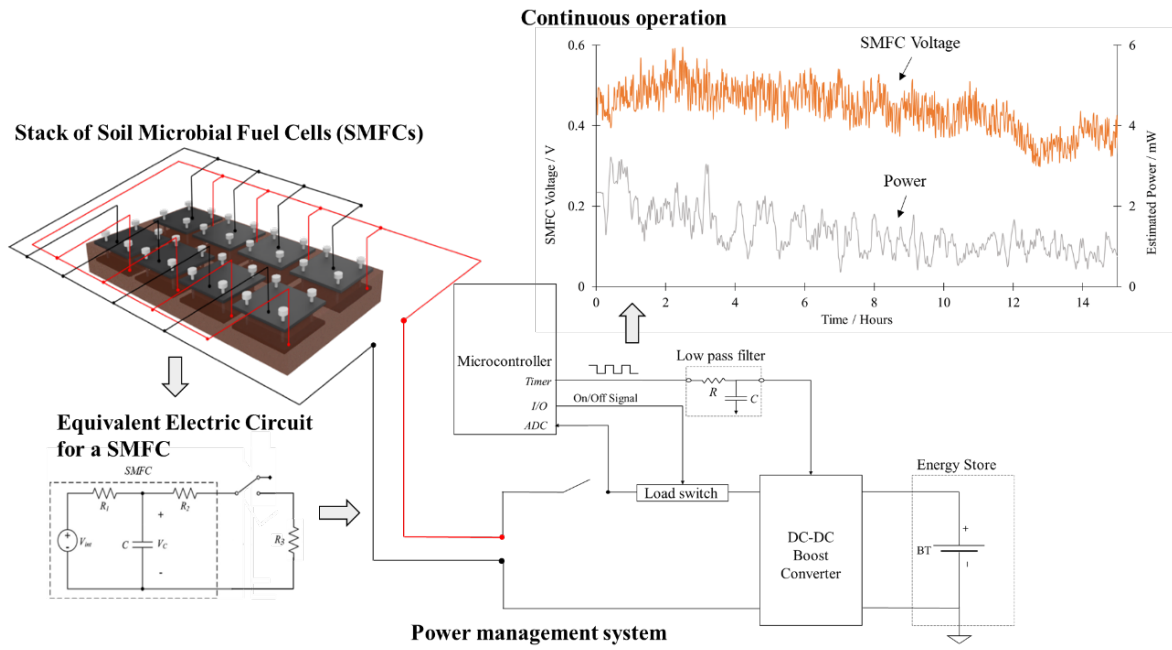
Keywords: Soil Microbial Fuel Cells; Equivalent Electrical Circuit; Maximum Power Point Tracking; Bioenergy

1. Introduction

Recent advancements in the renewable energy sector have sparked interest in developing off-grid and decentralised renewable energy systems (1). These small-scale energy generation units produce power near the point of use, making them more reliable and resilient compared to the centralised energy sources, and are particularly attractive in locations where conventional energy supply is restricted (2). Currently, wind and solar technologies are the top decentralised renewable energy contenders. Hybrid systems rather than reliance on a single power source, however, can enhance efficiency, reliability, and economics of such renewable power generation technologies (3). As both wind and solar based systems heavily rely on the environmental conditions, a technology less dependent on these factors, yet widely accessible, is desirable. In this context, Soil Microbial Fuel Cell (SMFC) technology holds potential as both a low-cost and sustainable power source (4). SMFC technology relies on endogenous electroactive microorganisms to convert the chemical energy stored in biodegradable matter in soil directly into electricity (5). Amongst the different types of microbial fuel cells, SMFCs are arguably the most cost attractive, as they utilise soil as the supporting matrix, the source of microorganisms, and, in membrane-less configurations, also as the separator between the anode and the cathode. Consequently, the overall system design is simplified and so is its operation, with no need for continuous fuel or oxygen pumping (6). Similarly to traditional microbial fuel cells, practical applications of SMFCs are hindered by difficulties on effective power scale-up strategies and long-term stability (7). Compared to other renewable energy technologies, microbial fuel cells are considered low power due to their inherent thermodynamic limitations. The electromotive force induced by the bioelectrochemical reactions that take place within the fuel cell is in fact limited to a theoretical maximum potential of 1.14 V, resulting in power densities in the range of tens to hundreds mW m^{-2} (6, 8, 9).

Several strategies to relieve physical and chemical constraints of singular SMFCs have been reported, which focus on the selection of optimal electrode materials, modification of the system architecture and optimisation of the operational conditions (7). These include the use of a silicone gas-diffusion cathode (9), and the incorporation of membranes, including the use of low-cost separators, such as terracotta (10). Oxygen crossover, high internal losses and poor proton diffusion, potentially due to biofouling (11) are key limitations in these studies.

To maximise the energy harvesting efficiency and achieve the voltage requirements for low-power electronics, the use of a power management system (PMS) is necessary (12). In particular, the impedance of the electrical load must match the internal resistance of the fuel cell to effectively convert the theoretical cell potential into practical power outputs (13).

Typically, the applied external electrical load in microbial fuel cells is pre-defined and the performance is maintained with the use of hysteresis controllers (14-16). This strategy relies on set voltage bands that need to be regularly updated and re-defined to account for any changes in the bioelectrochemical performance, which in turns requires frequent and time-consuming electrochemical analyses on the fuel cells (17). To overcome the issue of frequent operational disruptions, and facilitate practical applications, an active hysteresis control-based PMS has been recently proposed, which uses digitally controlled potentiometers for a real time maximisation of power. The high-energy demand of the potentiometer required, however, poses concerns on the net energy balance of the system (12). Model-based power estimation strategies could be the solution. These methods rely on equivalent electrical circuit (EEC) models, designed to replicate the dynamic behaviour of the SMFCs, from which electrochemical parameters (e.g. the internal resistance) can be derived and used to estimate the output power, without the need for direct measurements with a potentiometer or ammeter. Coronado et al proposed an EEC for microbial

fuel cells operated with pulse-width modulated electrical load, which enabled on-line parameter estimation of the internal resistance, capacitance, and open circuit voltage (OCV). A similar model was used to demonstrate the possibility of real-time maximum power adaptations under limiting and non-limiting organic load conditions, by intermittently connecting and disconnecting the applied load (18). Recently, a novel and energy efficient power estimation strategy has been proposed, which is based on a EEC that more accurately models the dynamics of a single conventional (i.e. liquid) microbial fuel cell (19). Nonetheless, the functionality of the tracking algorithm was presented only for a limited time, with no attempt to investigate the consequences of tracking the maximum power of the fuel cell in the long-term (20).

In this work, an effective EEC model is developed and applied for the first time to soil-based microbial fuel cells to generate practical solutions for energy harvesting. A maximum power point tracking algorithm is also developed and its effect on continuous operations assessed. The scalability and feasibility of this model on stacks of multiple SMFCs is also investigated. By setting the basis for effective energy harvesting strategies, this study paves the way for practical implementations of the SMFC technology.

2. Materials and methods

2.1. Materials

The soil used in the study was collected from the University of Bath campus. After collection, it was manually sieved and cleaned of small stones, roots, and leaves. Table 1 summarises the properties of the soil used. The nitrogen (N), phosphorous (P) and potassium (K) content in the soil was qualitatively assessed with the HI-3869 Soil Test Kit (Hanna Instruments) and quantified using a soil test interpretation guide (21). The pH and conductivity of the soil were measured by

using a Thermo Scientific Orion Star A325 probe. The initial water content of the soil, WC_{soil}, was determined from the weight difference before and after a drying process, according to Equation 1:

$$WC_{soil}(\%) = \left(\frac{W_1 - W_2}{W_2}\right) * 100\% \hspace{2cm} (1)$$

where, W_1 and W_2 is the weight (g) of the soil sample respectively before and after being oven-dried overnight at 105°C (22).

The organic matter content (OM%) of dried soil samples was analysed by the Loss of Ignition (LOI) method (23). Briefly, the samples where were heated to 375°C for 24 hours and the OM% was calculated according to Equation 2:

$$OM\% = \left(\frac{W_b - W_a}{W_b}\right) * 100\% \hspace{2cm} (2)$$

where W_b and W_a is the weight (g) of the soil sample respectively before and after ignition.

Table 1. Physiochemical properties of the soil used in the study.

Parameter	Value
pH	6.5
Nitrogen	Low: < 10 ppm
Phosphorous	Trace: < 10 ppm
Potassium	Low: < 150 ppm
Moisture Content	55 %
Organic Matter Content	20 ± 1.5 %

2.2. SMFC construction and operation

The SMFCs used in this study consisted of two graphite felt electrodes (10 x 10 x 0.7 cm), separated from each other with nylon screws (Bluemay Ltd) at a fixed distance of 4 cm, as previously described (6). The cathode was exposed to air, whilst the anode was buried in the soil. Before use, the anode underwent acid and heat treatment to increase hydrophilicity and roughness of the carbon nanofibers (24). The electrodes were connected to an external resistance by means of a titanium wire (0.25 mm diameter) manually woven through them. No external membrane was used to separate the electrodes.
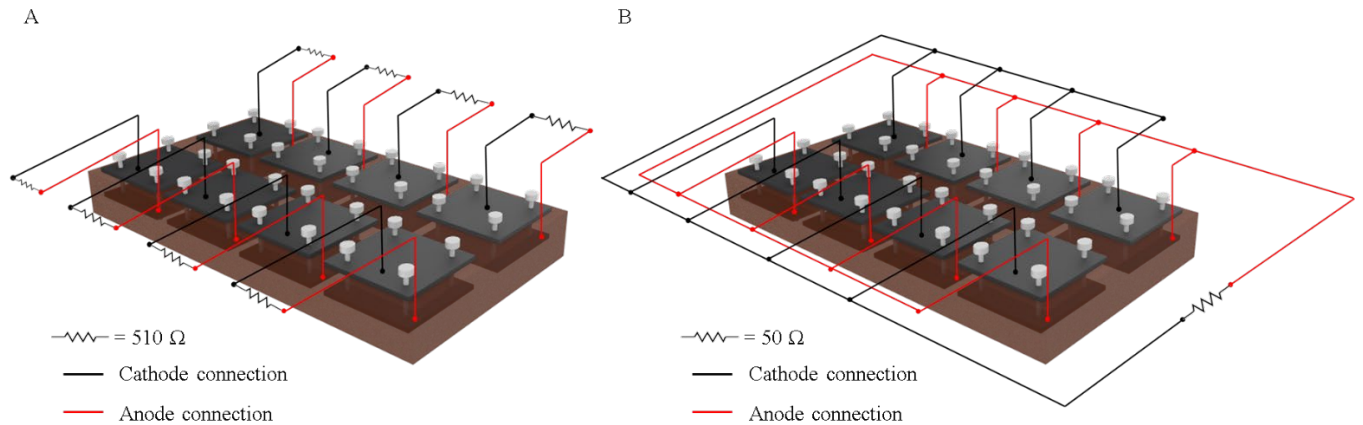

Figure 1. Soil microbial fuel cell arrangements tested in this study. A) Box 1: 8 SMFCs connected to individual external resistors. B) Box 2: stack of 8 SMFCs connected in parallel.

Sixteen SMFCs were constructed and distributed in two boxes (71 x 44 x 23 cm) filled with soil, as shown in Figure 1. To assess the most effective and practical route for stacking and operating the SMFCs, two different approaches for the electroactive bacteria enrichment process were tested. In one case (Box 1, Figure 1A), the eight SMFCs were enriched with an individual connection to an external load, R_{ext}, of 510 Ω; the fuel cells were electrically stacked together only

once the enrichment process was deemed completed. In the second case (Box 2), the SMFCs were instead electrically stacked in parallel from the very beginning of their operation and connected to a R_{ext} equal to 50 Ω. These values of R_{ext} were selected to facilitate the enrichment of electroactive bacteria by closely matching the internal resistance (R_{int}), according to previous results (6).

The SMFCs were operated at room temperature (20 ± 2 °C) and the output voltage, E, was monitored over time using a data acquisition system (DAQ6510, Keithley). Every two days, approximately 1.5 L of tap water was distributed amongst the two boxes via a gravity irrigation system, comprising of a 25 L water tank (TanksDirect), an electronic water timer (Kingfisher) and a micro drip irrigation kit (Yikaich).

The modified Gompertz model was used to interpolate the output voltage monitored versus time during the enrichment stage (24). Once a steady voltage output was observed (after approximately one month), the SMFCs underwent a series of polarization tests. The latter were performed by varying the applied resistance, R_{ext}, from 900 kΩ to 40 Ω every 10 minutes, by means of a resistance box (Cropico RM6 Decade) and recording the pseudo-steady output potential. Ohm's law, $E=I\,R_{ext}$, was used to calculate the corresponding current (I) at each value of R_{ext}. The power, P, was calculated using the power law, $P=IE$. The internal resistance was calculated by fitting the power curves with a polynomial trend line, extrapolating the data, and applying Jacobi's law, stating that $R_{int}=R_{ext}$ at the maximum power point (25).

2.3. SMFC equivalent circuit

Three EECs were used to model the SMFC, according to previous work on conventional (i.e. liquid) microbial fuel cells (20). The simplest model, Model 1 in Figure 2a, is a voltage source resistance circuit, where V_{int} is the internal voltage and R_{int} is the internal resistance of the SMFC. Model 2, shown in Figure 2b, describes the SMFC as a first order system, defined by only one

energy storage unit. The model includes a resistor-capacitor (RC) circuit, where C_{dl} is the double-layer capacitance, and R_1 and R_2 refer respectively to the ohmic losses and the charge transfer losses. Finally, Model 3, corresponding to the equivalent circuit proposed by Alaraj et al. (19), is a variation of the first order RC system in Model 2, and is characterised by a parallel double-layer capacitance and series resistances (Figure 2c). In Model 3, R_1 and R_2 represent the rate limiter for metabolic electron production (charge transfer losses) and current (ohmic losses), respectively (19).

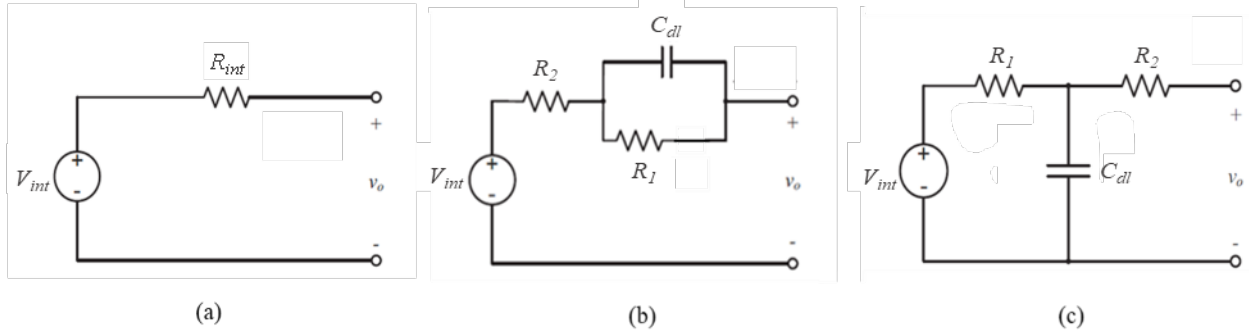(a)   (b)   (c)

Figure 2. Equivalent circuits used in this study to describe the electrical equivalent circuit of the SMFC. (a) Model 1: simplest equivalent circuit. (b) Model 2: conventional equivalent circuit. (c) Model 3: equivalent circuit proposed by Alaraj et al. (19).

To identify the model parameters, a series of polarisation tests, followed by open circuit tests were performed, following previous work (20). Data were recorded with a 1 s sampling period.

V_{int} was obtained by disconnecting the SMFC from the external load (R_{ext}), for t→∞ and by measuring the stable open circuit voltage.

R_2 (Ω) was calculated as:

$$R_2 = \frac{V^+ - V^-}{I} \qquad (3)$$

Where: V^+ (V) is the cell voltage registered right after opening the circuit; V^- (V) is the output voltage generated by the SMFC connected to an external load right before opening the circuit; I (A) is the current measured under closed circuit conditions.

R_1 (Ω) was calculated as:

$$R_1 = R_{int} - R_2 \qquad (4)$$

Where: R_{int} (Ω) is the total internal resistance extracted from polarization tests, as mentioned in the previous section.

Since the relation between the terminal voltage and the voltage across the internal double-later capacitor is identical, and increases in an exponential fashion up to the internal thermodynamic voltage, the capacitance, C (F), was calculated as:

$$C = \frac{-t}{\ln\left(\frac{V_C(t) - V_{int}}{V_C(0) - V_{int}}\right)} \qquad (5)$$

Where $V_{C(0)}$ is the capacitor voltage recorded 1 s after opening the circuit. $V_{C(t)}$ is the capacitor voltage sampled 40 s after opening the circuit, at approximately 63% of the OCV (the first time constant).

The so-calculated EEC parameters were input into a circuit design, and a simulation package (OrCAD, Cadence Design Systems), to model the electrical behaviour of the SMFCs and validate the experimental data.

2.4. Power Management System

In this study, two boost converter-based PMSs were constructed: an unmodified PMS and a modified PMS. Both systems consisted of a DC-DC boost converter (BQ22504, Texas Instruments), which steps up the input voltage from the SMFC (typically in the 300-600 mV range) to a desired voltage level and charges a 3.6 V 40 mAh NiMH battery used as a long-term energy store.

The inbuilt MPPT function of the BQ22405 boost converter was disabled in both PMSs, as originally developed for photovoltaic cells. Unlike solar cells, which reach a steady state OCV almost immediately after disconnecting the load, an SMFC can take anywhere from several minutes to hours. As a result, the short sampling time of the inbuilt MPPT (256 ms) would be insufficient to record a stable OCV value in a soil-based system.

2.4.1. Maximum Power Point Tracking

The modified PMS was customised with a MPPT algorithm. The algorithm was based on the Perturb and Observe (P&O) approach, which, by sampling terminal and capacitor voltages at a fixed operating point, calculates the proportional estimated power, P_{est}, as follows:

$$P_{est} = (V_C - V_T) \cdot V_T \qquad\qquad (6)$$

Where V_T (V) is the terminal voltage sampled right before opening the circuit and V_C (V) is the capacitor voltage measured 15 ms (minimum sampling time of the analogue digital converter) after the circuit is opened.

The operating point is changed according to the estimated power. After a sampling time of 100 s, selected to guarantee the achievement of a steady power output, a new operating point is measured, and the set-point voltage is adjusted in the direction that gives a higher power.

To enable continuous sampling of the parameters used for power estimations, a load switch (TPS22860, Texas Instruments) was used at the boost converter's input to connect or disconnect the BQ25504. The load switch was controlled by a microcontroller (NUCLEO-L010RB) that was programmed with the P&O algorithm, sampling and converting the analogue signal from the SMFC into its digital form, using an ADC, generating a reference voltage (V_{REF}). The digital signal was converted back to its analogue form with a low-pass filter and supplied to the boost converter to adjust the load impedance of the BQ25504, such that the voltage coming from the SMFCs (V_{in}) is equal to V_{REF}, which is the point of maximum power generation, as given by Jacobi's law. To guarantee safe and reliable operation, all the electronic components were placed in an IP67 box, designed to protect them from humidity and dust.

Figure 3 shows the electronic circuits of the two PMSs used in the study. The black lines represent the electronic circuit of the unmodified PMS, and the red lines show the modifications added, in the modified PMS.
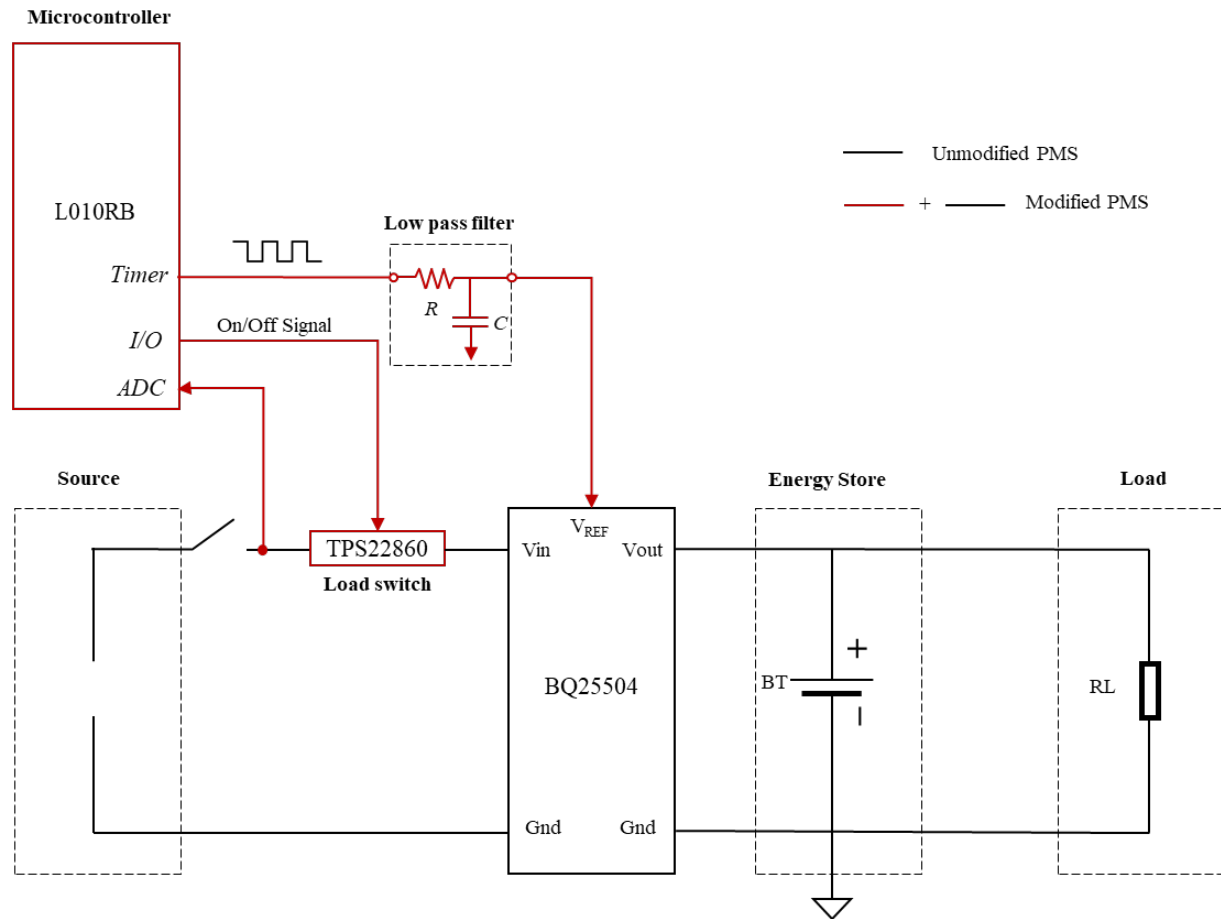
Figure 3. Electronic circuits of the power management systems used in this study. Black lines refer to the unmodified PMS circuit. Red lines represent the modifications added in the modified PMS.

3. Results and discussion

3.1. Enrichment of the SMFCs

Electrically stacking multiple microbial fuel cells is an effective strategy to scale-up the power generated with this technology (4). Typically, each fuel cell is operated individually and electrically stacked together only once a steady state output voltage is observed. While this

approach allows monitoring the performance of each fuel cell, stacking the fuel cells from the very beginning of operation is more practical. To investigate the effect that the latter approach may have on the overall performance the enrichment of eight individual SMFC units (Box 1) was investigated and compared with the enrichment of a stack of eight SMFCs electrically connected in parallel (Box 2). The results are shown in Figure 4.

When enriched individually, the SMFCs had a lag phase two times shorter than the SMFCs stack. This faster response could be a consequence of the difference in external load (R_{ext} = 510 Ω for each SMFC in Box 1 and 50 Ω for the stack in Box 2). It has been previously shown that the external load used during the enrichment has a direct effect on biofilm structure and properties (26). In particular, higher external loads promote faster acclimation of mix-cultured biofilm (27). From day 5 onwards, a less than 12 % difference was observed in the output voltage generated by the individual SMFCs and the SMFCs stack. After two weeks, the two systems generated a steady output voltage of 156 ± 13 mV (individual SMFCs, n = 8) and 166 mV (SMFCs stack).
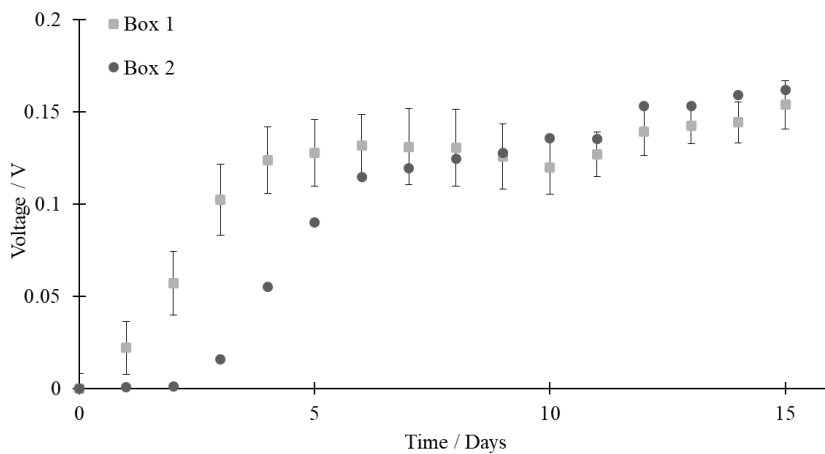
Figure 4. Enrichment of SMFCs operated in individual (Box 1) and in stacked (Box 2) mode. Error bars refer to 8 replicates for the case of individually connected SMFCs. The stack includes 8 SMFCs electrically connected in parallel.

Following the completion of the enrichment and after another two weeks of operation, the SMFCs stack was disassembled, and each fuel cell was connected to a R_{ext} of 510 Ω, to assess individual performance. Under these conditions, it resulted that the SMFCs enriched as a stack had an anode potential of -371 ± 15 mV, whereas the SMFCs connected to their own resistances from the start, had developed a higher anode potential, -301 ± 13 mV. This result suggests a better oxidation of the organic matter by the anodic biofilm for the case of the SMFCs enriched in a stack, with more electrons generated and transferred to the electrodes.

This hypothesis was further confirmed by polarisation tests. As shown in Figure 5 the SMFCs enriched as a stack generated a peak power 75% higher than the SMFCs individually enriched (0.84 ± 0.13 mW versus 0.47± 0.24 mW). Similarly, the peak current produced by the stack was almost double (2 mA versus 1.35 mA). This result could be the consequence of a different composition of electroactive species in the anodic biofilm in each case. High R_{ext} values promote the development of biofilms rich in extracellular polymeric substances, leading to looser structures and, hence, lower output current densities (28, 29). In contrast, operating at lower R_{ext}, leads to denser and more uniform biofilms with little extracellular polymeric substances content (30). This could be the reason why, under a more negative anode potential, smaller error bars and greater power densities were obtained with the SMFCs operated in stack under 50 Ω. Nonetheless, this test confirmed that the enrichment of the SMFCs can be performed directly in stack, thus simplifying practical implementations.
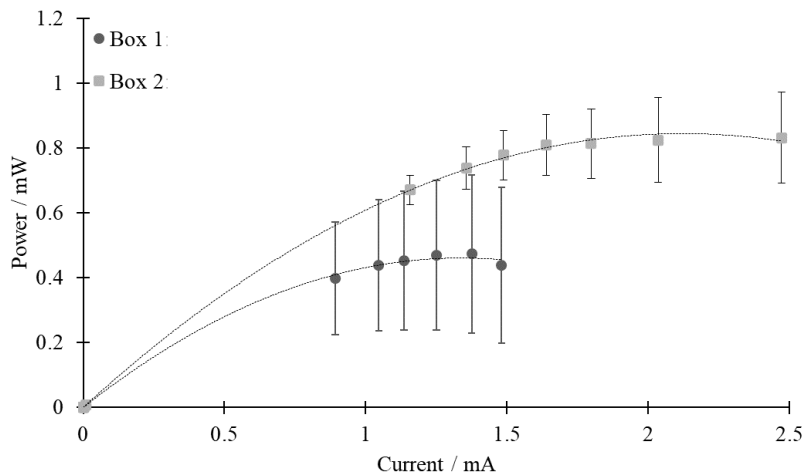
Figure 5. Comparison of power curves for the SMFCs in Box 1, enrichment of individual fuel cells, and Box 2, enrichment of 8 fuel cells connected in parallel. The polarisation tests were performed after 4 weeks of operation. Error bars refer to 8 replicates.

3.2. SMFC Equivalent Electrical Circuit

To develop an efficient model-based estimation of the electrochemical parameters and an effective power harvesting strategy for the SMFCs stack, it is important to model the electrical behaviour of the SMFC. Previous work has explored the use of different EECs to simulate both voltage and current dynamics of these systems (17, 19, 20), as shown in Figure 2. The accuracy of the proposed models has, however, only been tested on conventional (i.e. liquid) microbial fuel cells, operated as a single unit (i.e. not in a stack). Although soil-based microbial fuel cells share the same working principles as any other microbial fuel cell subclass, marked differences in reactor structure, microbial communities, and, most of all, electrolyte, demand for a validation of the EECs models previously proposed for liquid microbial fuel cells. Therefore, the feasibility of such models for the SMFC used in this study was tested. To ensure high accuracy and reproducibility,

the study was done on the 8 SMFCs from Box 2, which performed uniformly. A series of

polarisation tests and open circuit tests were carried out as described in Section 2.3, to identify the

model parameters summarised in Table 2. First, these tests were carried out on single SMFCs, then

on stacks of two, three and four SMFCs, to investigate the scalability of the parameters identified.

Table 2. Equivalent circuit parameters for single SMFCs and a stack of 2, 3 and 4 SMFCs, with
standard deviation referring to 8, 4, 2 and 2 replicates, respectively.

SMFC	V^+ mV	V^- mV	V_{int} mV	I mA	R_1 Ω	R_2 Ω	R_{int} Ω	C F
Single	692.5 ± 34.1	631.8 ± 42.8	846.7 ± 3.8	1.2 ± 0.1	149.7 ± 28.2	49.7 ± 11.4	199.3 ± 20.8	0.6 ± 0.17
2-stack	750.8 ± 9.6	713.3 ± 10.2	846.7 ± 4.3	1.4 ± 0.02	78.0 ± 7.2	26.8 ± 2.0	104.8 ± 6.9	1.0 ± 0.20
3-stack	772.5 ± 9.5	745.5 ± 8.5	837.8 ± 7.8	1.5 ± 0.02	51.2 ± 0.6	18.5 ± 0.5	69.7 ± 0.2	1.4 ± 0.14
4-stack	783.5 ± 1.5	768.0 ± 5.0	850.4 ± 6.1	1.5 ± 0.01	39.2 ± 2.4	10.3 ± 2.4	49.5 ± 0.0	1.7 ± 0.13

The extracted parameters were used to simulate the responses generated by the different

EECs for a single SMFC, and compared against the experimental data, as shown in Figure 6. Three

areas, where the model deviates from the experimental data, were identified and categorised as

$Zone_1$, $Zone_2$ and $Zone_3$ (corresponding to the three shades of grey in Figure 6). $Zone_1$ refers to the

terminal voltage (V_T) of the SMFC operated under a 510 Ω load, Zone$_2$ to the voltage transient

right after opening the circuit, and Zone$_3$ to the voltage increase with time, until OCV is reached.
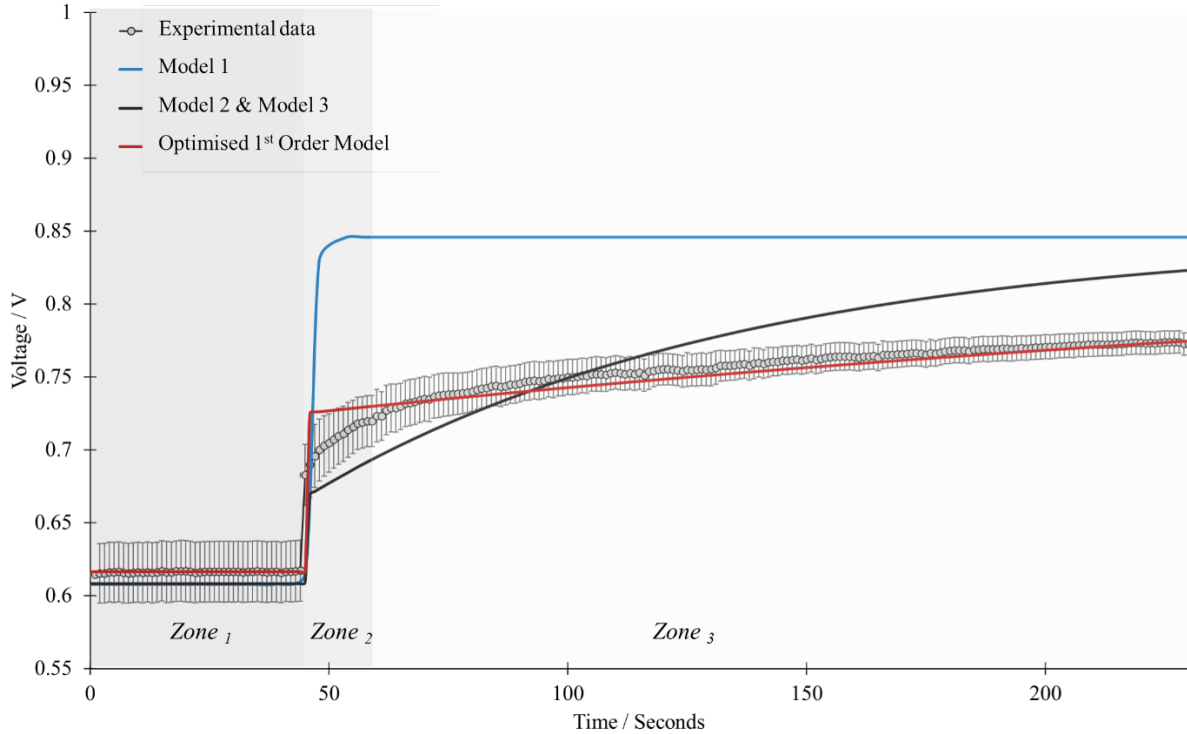

Figure 6. Experimental versus modelled data of the open circuit voltage dynamics in a single

SMFC. Error bars on data points refer to 8 replicates.

The voltage source resistance circuit in the EEC Model 1 showed the largest deviation from

the experimental SMFC voltage dynamics, with a correlation coefficient of 0.96. The major

inconsistencies between model and experimental data are related to Zone$_2$ and Zone$_3$, since,

according to the model, the SMFC reaches its full OCV almost immediately after disconnecting

the load. The internal dynamics of the SMFC are not therefore adequately modelled. Consequently,

many MPPT algorithms that are based on similar EECs (including the in-built MPPT tracker in

BQ-25504) are sub-optimal (31).

To represent the exponential rise in terminal voltage associated with the bioelectrochemical processes occurring in the SMFC, both Model 2 and Model 3 incorporate a first-order exponential function via a resistor connected with an energy storage element in the form of a capacitor. The different arrangement of electrical components in Model 3 allows a better modelling of the internal anodic electron flow and double-layer charge storage characteristics, as compared to Model 2 (19). Nonetheless, since the electrochemical parameters for both models, obtained from Equations 3-5, were the same, no differences between Model 2 and Model 3 were noted.

Both first-order EECs, gave a correlation coefficient of 0.97 with the experimental data. As shown in Figure 6, the models are characterised by a slow charge rate in $Zone_2$, which is controlled by the charge transfer resistance. From an electrical circuit standpoint, resistor R1 or R2 (according to whether Model 2 or Model 3 is used respectively), controls the rate at which the capacitor is charged and discharged. The higher the resistance, the slower the charge time and vice versa, indicating that the charge transfer resistance of 149.7 Ω may have been overestimated Furthermore, the time to reach OCV is underestimated by the two models, as Model 2 and Model 3 reach a value of 823 mV (97% OCV) at the end of $Zone_3$, which is 50 mV higher than the value observed experimentally. This result suggests that the 0.6 F capacitance is too low. By optimising the model parameters, lowering the charge transfer resistance to 100 Ω and increasing the capacitance to 3.5 F, a correlation coefficient of 0.988 was reached (Optimised First-Order Order Model fit in Figure 6), which is the best attainable fit with the proposed first-order EEC.

Following the completion of the parameter identification tests on individual SMFCs, the same analysis was then carried on the stack of two, three and four SMFCs, as shown in Figure S1 in the Supplementary Data. The tests revealed that the theoretical capacitance linearly increases with the number of SMFCs in a stack, as shown in Figure S2. This trend is expected, considering

that the capacitance is related to plate/electrode area, thus the value of capacitors connected in parallel is equal to the sum of all individual capacitances, according to Equation 8:

$$C_{Total} = C_1 + C_2 + C_3 \qquad (8)$$

Similarly, the resistance values R_1 and R_2 for the SMFC stacks follows the exponential decay trend of the internal resistance, according to Equation 9 (See Figure S3). These trends could therefore be used to predict the equivalent circuit parameters for larger SMFC stacks, becoming an important means for effective scale-up strategies for energy harvesting.

$$R_{Total} = \frac{1}{R1} + \frac{1}{R2} + \frac{1}{R3} \qquad (9)$$

The same deviations observed in $Zone_2$ and $Zone_3$ when modelling individual SMFCs, were observed also for the SMFC stacks, thus confirming the difficulty to precisely model SMFC voltage dynamics with first-order circuits. A second-order exponential RC model was thus considered, in which the terminal voltage follows Equation 10 (32):

$$V(t) = V_{OC} - IR_1 e^{-\frac{t}{\tau_1}} - IR_2 e^{-\frac{t}{\tau_2}} \qquad (10)$$

where $\tau_1 = R_1 C_1$, $\tau_2 = R_2 C_2$ represent two time-constants. Accordingly, Equation 10 can be rewritten as:

$$V(t) = V_{OC} - ae^{-bt} - ce^{-dt} \qquad (11)$$

Non-linear optimisation was performed using MATLAB (MathWorks) to minimise the difference between the modelled and experimental data, leading to a significantly improved graphical fit and a correlation coefficient of 0.998 (Figure 7). This result confirms that a second-order EEC model is a better fit to the experimental data. Gatti et al have previously derived a simple second-order EEC model to describe a liquid microbial fuel cell (33). Although the relative

error coming from cross validating the estimated parameters remained below 28%, their proposed model required knowledge on the substrate concentration near the anode region, which can be difficult to obtain for systems with a complex substrate composition such as SMFCs. Therefore, efforts should go into establishing a model that: 1) is based on simple measurements, 2) is described by bioelectrochemical and physical variables and parameters, 3) has low computational needs.
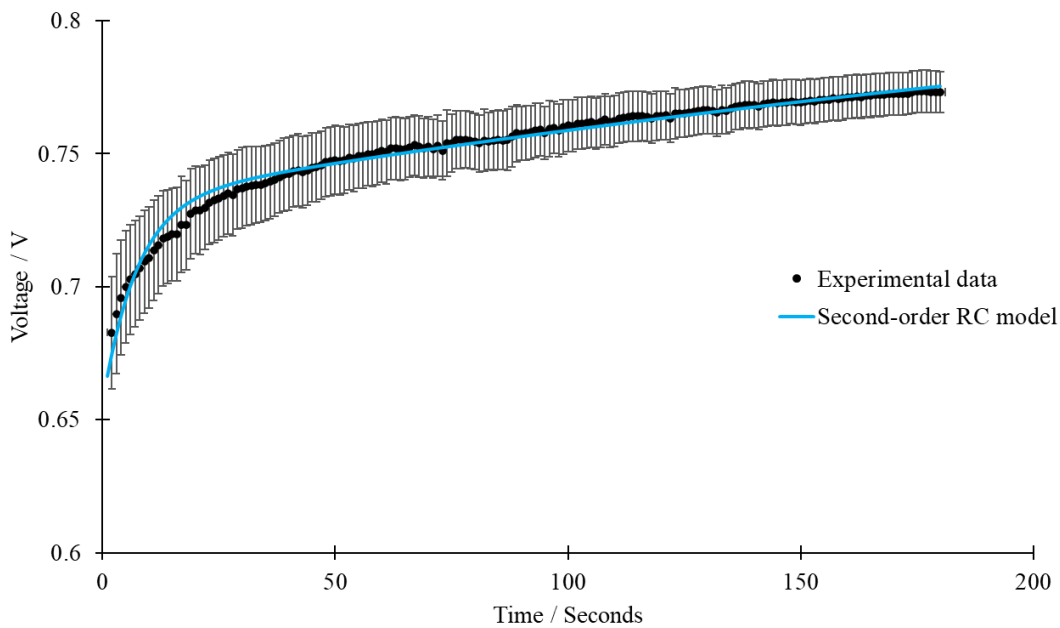

Figure 7. Second-order resistor-capacitor circuit model to fit experimental data. Error bars refer to 8 replicates. The model was obtained by running a non-linear optimisation routine in MATLAB.

3.3. Maximum Power Point Tracking

The design of an effective maximum power point tracking strategy is critical to improve the efficiency of the SMFCs stack, while substantially reducing volume and cost requirements of an up-scaled system. In this study, the effectiveness of the P&O method, proposed by Alaraj et al.

(20), in tracking the maximum power point of the SMFCs in continuous operations, was assessed. With this purpose, two stacks of 4 SMFCs each, referred to as Stack 1 and Stack 2, were connected respectively to a PMS modified with the P&O algorithm and a PMS without any modifications and thus no MPPT. Figure 4S shows the electrochemical characterisation of the two stacks; Stack 1 and Stack 2 generated a maximum power of 4.6 and 4.7 mW, respectively, while the polarisation tests revealed an internal resistance for both stacks of approximately 49.5 Ω.

Stack 1 was connected to the modified PMS, equipped with the MPPT function, and Stack 2 was connected to the unmodified PMS without MPPT. Both systems were left to charge a 3.6 V 40 mAh NiMh battery for 25 Hours. Figure 8A shows the output voltage of the two stacks during the charge test. The voltage generated by Stack 2 dropped by approximately 100 mV right after the start and was maintained at around 730 mV for the entire duration of the test. From the polarisation studies (Figure 4S), it can be deducted that the energy harvester applied a resistance of approximately 400 Ω, under which the SMFCs generated 1.3 mW of power at 1.8 mA of current, which corresponds to 28% of the maximum power.
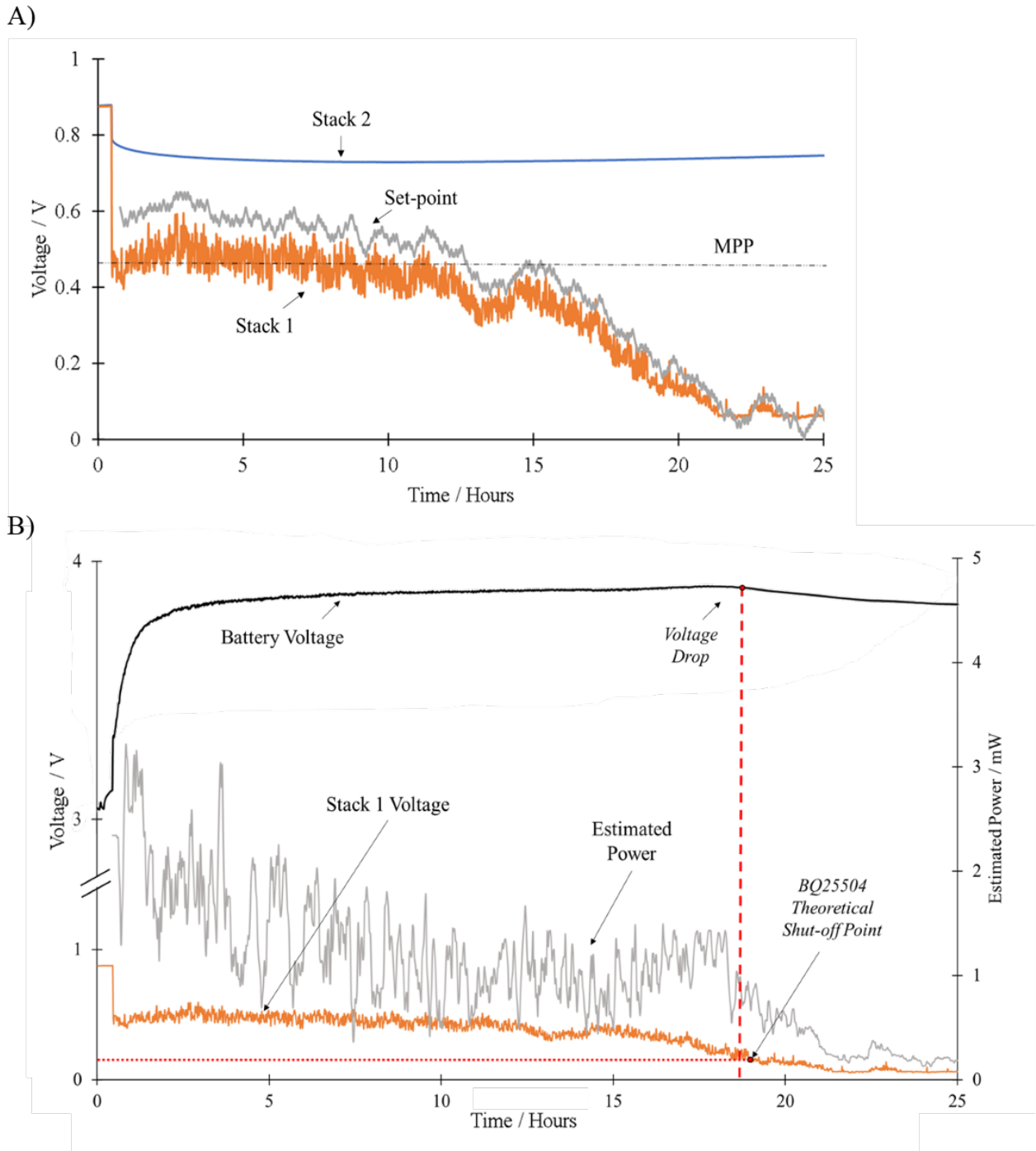
Figure 8. (A) Performance comparison of Stack 1, connected to the modified PMS, and Stack 2, connected to the unmodified, equipped with and without the MPPT algorithm, respectively; (B) Power estimates obtained by the P&O algorithm, along with the voltage generated by Stack 1 and the battery voltage, during operation.

The output voltage generated by Stack 1 followed the set-point imposed by the P&O algorithm, which demonstrates the successful adaptation of the MPPT method in the modified PMS. The slight differences in the set-point values versus the actual SMFC output voltage are most likely a consequence of ADC errors (the ADC internal to the microcontroller was referenced to the 5 V supply and had limited resolution). Nonetheless, such differences are insignificant in a P&O algorithm, as the role of the set-point is to adjust the resistance to either a higher or a lower value, thus it is the directional information that is relevant.

During the first 12 hours, Stack 1 generated an average output voltage of 450 ± 50 mV, corresponding to approximately 4.1 mW and 9.4 mA, which is equivalent to 90% of the maximum power point. After 15 hours, the output voltage began to drop, reaching values below 100 mV after 22 hours of operation. The cause for this drop might be related to a phenomenon known as voltage overshoot (34); when high current is extracted from microbial fuel cells, the anode and cathode potential can change from negative to positive and vice versa, thus reducing the voltage, and the output power. Sample points of the anode potential at time 0 h and 25 h demonstrated an increase from -400 mV to +60 mV vs. Ag/AgCl. This increase suggests that the anode is responsible for the performance decay, since the cathode potential was steady at about 50 mV vs. Ag/AgCl. This drop in the anodic performance could be caused by dynamic changes in the biofilm when exposed to lower resistances. Incorporating a MPPT into a stack of microbial fuel cells may lead to increased oxidation rates of the carbon-energy substrate at the anode, which in turn results in higher microbial growth rates and hence biomass density (27). In a continuous flow-through system, the thickness of the biofilm can be controlled, as the outer layers in loose contact with the electrode are constantly washed out (27). On the other hand, a significantly thick biofilm can build-up at the anodes of the SMFCs, which can hinder charge transfer across the several biofilm layers

and increase the overall internal resistance (35). Besides, microorganisms cannot sustain high voltages and elevated stack currents (36). It has been observed that, when forced to generate currents beyond their metabolic capacity, the electroactive bacteria become dysfunctional and collapse (37). Finally, high stack currents can turn biofilms acidic; the pH drop is a result of proton accumulation in the anodic region, due to slower transfer kinetics, weakening the biofilm and reducing the overall performance (38).

Fuel limitation may be another reason for the decay in the anode performance, considering that these tests were carried out after 90 days of operation of the SMFCs in batch mode (39). During this time, each SMFC converted approximately 3.3 kJ of chemical energy stored in organic matter into electrical energy, dissipated into a fixed external resistance. Furthermore, running at maximum power point increases the substrate consumption rate by the microbes (40), which in turn would deplete the available sources much faster. On the other hand, this decay was not observed for Stack 1, which operates at 28% of its maximum capability (27). An in-depth investigation on the nature of the organic matter in soil and any change over time, along with metabolomic analyses of the anodic biofilm, should be performed in future work, to better prove the hypothesis of fuel decay or change in its availability. Such study may also lead to the conclusion that a fed-batch operation, in which target nutrients are regularly supplied to the system, is an essential strategy to extend the duration of active energy harvesting at maximum power point.

The proposed P&O algorithm accounted for the changes in the bioelectrochemical performance. Figure 8B shows the 5-point moving average of the estimated power during the 25-hour operation. While these values are estimates and do not necessarily reflect the actual power generated by the SMFCs, they provide a clear indication on trends. The large fluctuations in power are most likely a consequence of the poor resolution of the ADC converter and should be addressed

in future work by using an ADC with a larger resolution. Once the voltage generated by Stack 1 dropped below 160 mV, a more rapid decay in the estimated power was observed. Interestingly, at the same time, the battery voltage dropped. Since the BQ25504 boost converter extracts power down to a minimum input voltage of 130 mV, it is very likely that the PMS system shut down when the stack voltage approached this limit (41). This interruption might in turn have interfered with the accuracy of the P&O algorithm, as the microcontroller was no longer able to control the boost converter. A possible solution to this problem could be to set control bands on the voltage generated by the SMFCs, which would prevent the voltage to drop below a threshold value.

As summarised in Table 3, our work reports one of the longest active-MPPT demonstrations on a microbial fuel cell system. It is also the first study done on a soil-based system. While there have been studies on operations lasting from 1 up to 62 weeks, details on the MPPT strategy implemented have not been provided, which prevents comparisons with previous work (39, 42). The model-based approach we propose in this study is particularly attractive, as it offers active tracking, since it does not rely on electrochemical methods, such polarization curves, cyclic voltammetry, and electrochemical impedance spectroscopy to determine the maximum power point. Consequently, there is no need for external analytical tools, which are time consuming and require specialised equipment (i.e. potentiostats). Furthermore, unlike the hysteresis-controlled operation, where the energy harvesting strategy is split into charge/discharge cycles, the model-based approach proposed in this study offers an advantage of continuous and non-disruptive power extraction from the SMFCs stack.

Table 3. Summary of studies reporting the use of MPPT in boost converter-based energy harvesting systems for microbial fuel cells.

Harvesting strategy	Type of fuel cell	Scale	MPPT strategy	Duration	Ref
Discharge/Charge	Liquid-based	Single	Hysteresis control	30 min	(14)
Discharge/Charge	Liquid-based	Single	Hysteresis control	25 min	(15)
Discharge/ Charge	Liquid-based	Single	Hysteresis control	18 h	(16)
Continuous	Liquid-based	Single	Hysteresis control + P&O	40 min	(43)
Continuous	Liquid-based	Single	P&O	1.2 h	(44)
Continuous	Soil-based	Stack	P&O	25 h	This work

4. Conclusions

In this work, effective solutions for scale-up and operation of soil microbial fuel cell technology are investigated. Maturing the biofilm by stacking the SMFCs from the start of operation resulted to be an effective and practical strategy, with 75% higher power densities, compared to SMFCs that were enriched individually. Following the enrichment studies, a perturbation/observation MPPT algorithm, based on a more energy efficient power estimation strategy, was tested on the SMFC stacks. Battery charge tests revealed that operating the stacks with a power management system featuring the MPPT algorithm extracted more than three times the power, as opposed to running the system without the MPPT. A more in-depth analysis of the equivalent electrical circuit models, on which the P&O algorithm was based, revealed that a second-order function improves the model fit and will allow for further optimisation of the power harvesting solutions. Finally, long-term studies revealed that operating the fuel cells near the maximum performance led to a power decay after 18 hours of operation. Although the exact cause

for the performance drop remains unclear, the electrode potentials confirmed that the voltage decrease was related to a significant increase in anode potential.

5. Acknowledgements

6. References

1.   Wolfe P. The implications of an increasingly decentralised energy system. Energy Policy. 2008;36:4509-13.

2.   Alstone P, Gershenson D, Kammen DM. Decentralized energy systems for clean electricity access. 2015.5:305-14.

3.   Bajpai P, Dash V. Hybrid renewable energy systems for power generation in stand-alone applications: A review. 2012;16(5):2926-39.

4.   Logan BE. Microbial Fuel Cells: Wiley; 2007.

5.   Santoro C, Arbizzani C, Erable B, Ieropoulos I. Microbial fuel cells: From fundamentals to applications. A review. Journal of Power Sources. 2017;356:225-44.

6.   Dziegielowski J, Metcalfe B, Villegas-Guzman P, Martinez CA, Gotrayeb A, Wenk J, et al. Development of a functional stack of soil microbial fuel cells to power a water treatment reactor: From the lab to field trials in North East Brazil. Applied Energy. 2020;278.

7.   Flimban SGA, Ismail IMI, Kim T, Oh S. Overview of Recent Advancements in the Microbial Fuel Cell from Fundamentals to Applications: Design, Major Elements, and Scalability. Energies. 2019;12.

8.   Ren H, Chae J. Fuel cells technologies for wireless MEMS. Wireless MEMS Networks and Applications. 2017.

9.   Wetser K, Dieleman K, Buisman C, Strik D. Electricity from wetlands: Tubular plant microbial fuels with silicone gas-diffusion biocathodes. Applied Energy. 2017;185:642-9.

10.   Casula E, Kim B, Chesson H, Lorenzo MD, Mascia M. Modelling the influence of soil properties on performance and bioremediation ability of a pile of soil microbial fue cells. Electrochimica Acta. 2021;368.

11.   Ezziat L, Elabed A, Ibnsouda S, Abed SE. Challenges of Microbial Fuel Cell Architecture on Heavy Metal Recovery and Removal From Wastewater. frontiers in Energy Research. 2019.

12.   Park J, IEEE, Ren Z. Hysterersis-Controller-Based Energy Harvesting Scheme for Microbial Fuel Cells With Parallel Operation Capability. IEEE Transactions on Energy Conversion. 2012;70.

13.   Papaharalabos G, Strinchcombe A, Horsfield I, Melhuish C, Greenman J, Ieropoulos I. Autonomous Energy Harvesting and Prevention of Cell Reversal in

MFC Stacks. Journal of The Electrochemical Society. 2017;164(3).

14.   Park J, Ren Z. High efficiency energy harvesting from microbial fuel cells using a synchronous boost converter. Journal of Power Sources. 2012;208:322-7.

15.   Alaraj M, Ren ZJ, Park J. Microbial fuel cell energy harvesting using synchronous flyback converter. Journal of Power Sources. 2014;247:636-42.

16.   Wang H, Park J, Ren Z. Active Energy Harvesting from Microbial Fuel Cells at Maximum Power Point without Using Resistors. Environmental Science & Technology. 2012;46:5247-52.

17.   Coronado J, Tartakovsky B, Perrier M. On-line monitoring of microbial fuel cells operated with pulse-width modulated electrical load. Journal of Process Control. 2015;35:59-64.

18.   Coronado J, Perrier M, Tartakovsky B. Pulse-width modulated external resistance increases the microbial fuel cell power output. Bioresource Technology. 2013;147:65-70.

19.   Park J, Roane TM, Ren ZJ, Alaraj M. Dynamic modeling of a microbial fuel cell considering anodic electron flow and electrical charge storage. Applied Energy. 2017;193:507-14.

20.   Alaraj M, Park J. Net power positive maximum power point tracking energy harvesting system for microbial fuel cell. Journal of Power Sources. 2019;418:225-32.

21.   Horneck DA, Sullivan DM, Owen JS, Hart JM. Soil Test Interpretation Guide. Oregon State University2011.

22.   Jim R, Mike M. Moisture content by the oven-dry method for industrial testing. Oregon State University, Corvallis, OR1999.

23.   Konare H, Yost R, Doumbia M, Mccarty GW, Jarju A, Kablan R. Loss of ignition: Measuring soil organic carbon in soils of the Sahel, West Africa. African journal of agricultural research. 2010;5(22):3088-95.

24.   Monasterio S, Lorenzo MD. Electricity generation from untreated fresh digestate with a cost-effective array of floating microbial fuel cells. Chemical Engineering Science. 2019;198:108-16.

25.   G. Papaharalabos, Stinchcombe A, Horsfield I, Melhuish C, Greenman J, Ieropoulos I. Autonomous Energy Harvesting and Prevention of Cell Reversal in MFC Stacks. Journal of The Electrochemical Society. 2017;164:3047-51.

26.   Liu T, Yu Y, Li D, Song H, Yan X, Chen WN. The effect of external resistance on biofilm formation and internal resistance in Shewanella inoculated microbial fuel cells. RSC Advances. 2016(24).

27.   Pasternak G, Greenman J, Ieropoulos I. Dynamic evolution of anodic biofilm when maturing under different external resistive loads in microbial fuel cells. Electrochemical perspective. Journal of Power Sources. 2018;400:392-401.

28.   Dennis PG, Virdis B, Vanwonterghem I, Hassan A, Hugenholtz P, Tyson GW, et al. Anode potential influences the structure and function of anodic electrode and electrolyte-associated microbiomes. Scientific reports. 2016;6.

29.   Commault AS, Lear G, Packer MA, Weld RJ. Influence of anode potentials on selection of G*eobacter* strains in microbial electrolysis cells. BioSource Technology. 2013;139.

30.   Zhang L, Zhu X, Li J, Liao Q, Ye D. Biofilm formation and electricity generation of a microbial fuel cell started up under different external resistances. Journal of Power Sources. 2011;196(15).

31.   Degrenne N, Buret F, Allard B, Bevilcqua P. Electrical energy generation from a large number of microbial fuel cells operating at maximum power point electrical load. Journal of Power Sources. 2012;205:188-93.

32.   Zhang L, Peng H, Ning Z, Mu Z, Sun C. Comparative Research on RC Equivalent Circuit Models for Lithium-Ion Batteries of Electric Vehicles. Applied Sciences. 2017;1002(7).

33.   Gatti MN, Milocco RH. A biofilm model of microbial fuel cells for engineering applications. International Journal of Energy and Environmental Engineering. 2017;8:303-15.

34.   Winfield J, Ieropoulos I, Greenman J, Dennis J. The overshoot phenomenon as a function of internal resistance in microbial fuel cells. Bioelectrochemistry. 2011;81(1):22-7.

35.   Campo AGd, Canizares P, Lobato JL, Rodrigo M, Fernandez-Morales FJ. Effects of External Resistance on Microbial Fuel Cell's Performance. In: Springer, editor. Environment, Energy and Climate Change II2014.

36.   Margaria V, Tommasi T, Pentassuglia S, Agostino V, Sacco A, Armato C, et al. Effects of pH variations on anodic marine consortia in a dual chamber microbial fuel cell. International Journal of Hydrogen Energy. 2017;42:1820-9.

37.   An J, Sim J, Lee H. Control of voltage reversal in serially stacked microbial fuel cells through manipulating current: Significance of critical current density. Journal of Power Sources. 2015;283:19-23.

38.   Yuan Y, Zhao B, Zhou S, Zhong S, Zhuang L. Electrocatalytic activity of anodic biofilm responses to pH changes in microbial fuel cells. Biosource Technology. 2011;102:6887-91.

39.   Fischer F, Sugnaux M, Savy C, Hugenin G. Microbial fuel cell stack power to lithium battery stack: Pilot concept for scale up. Applied Energy. 2018;230:1633-44.

40.   Zhang J, Zheng P, Zhang M, Chen H, Chen. T, Xie Z, et al. Kinetics of substrate degradation and electricity generation in anodic denitrification microbial fuel cells (AD-MFC). Bioresource Technology. 2013;149:44-50.

41.   Instruments T. BQ25504 Ultra Low-Power Boost Converter With Battery Management For Energy Harvester Applications. 2019.

42.   Blatter M, Delabays L, Furrer C, Huguenin G, Cachelin CP, Fischer F. Stretched 1000-L microbial fuel cell. Journal of Power Sources. 2021;483.

43.   Park J. Hysteresis controller based maximum power point tracking energy harvesting system for microbial fuel cells. Journal of Power Sources. 2012;205:151-6.

44.   Erbay C, Carreon-Bautista S, Sanchez-Sinencio E, Han A. High Performance Monolithic Power Management System with Dynamic Maximum Power Point Tracking for Microbial Fuel Cells. Environmental Science & Technology. 2014;48:13992-9.

Towards Effective Energy Harvesting from Stacks of Soil Microbial Fuel Cells
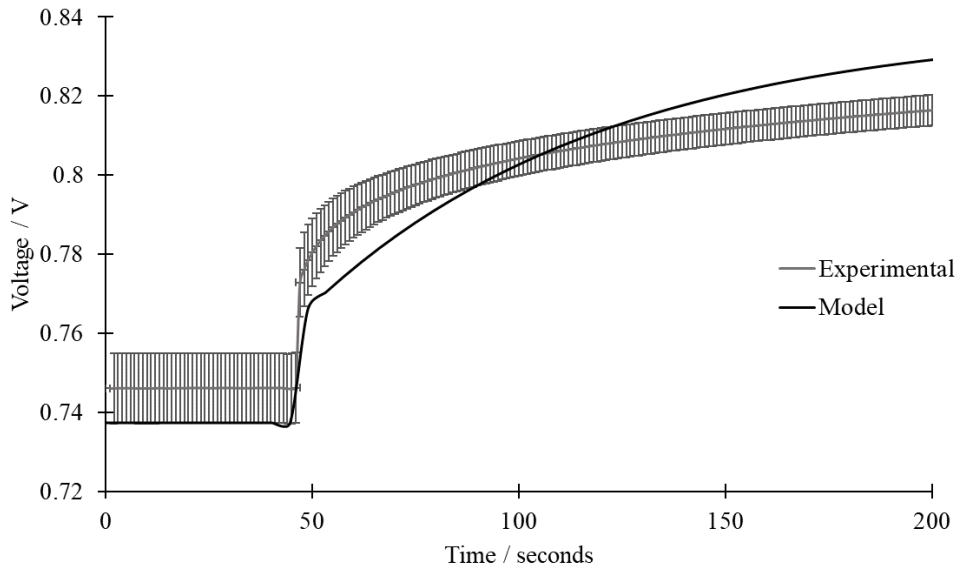
Jakub Dziegielowski[1,2], Benjamin Metcalfe[2,3], Mirella Di Lorenzo[1,2]*
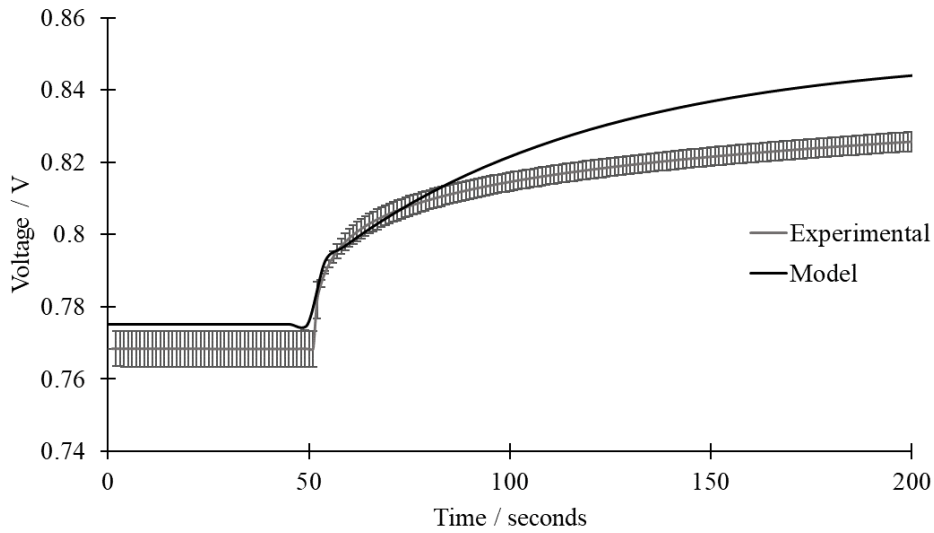
Supplementary Data

A)
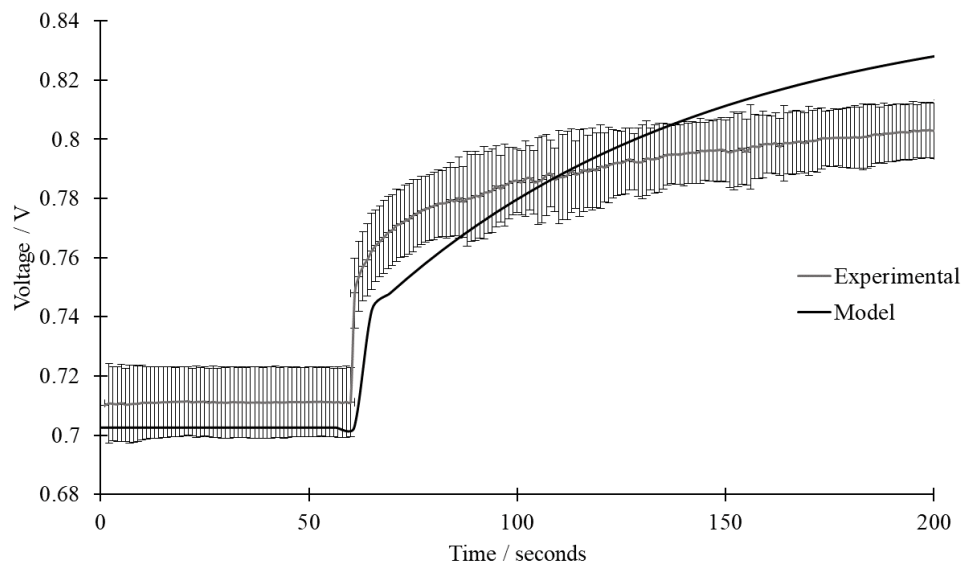
B)

C)

Figure 1S. Experimental versus modelled data of the open circuit voltage dynamics in a parallelly connected stack of: A) 2 SMFCs; B) 3 SMFCs; C) 4 SMFCs. Error bars refer to replicates of 4, 2 and 2, respectively.
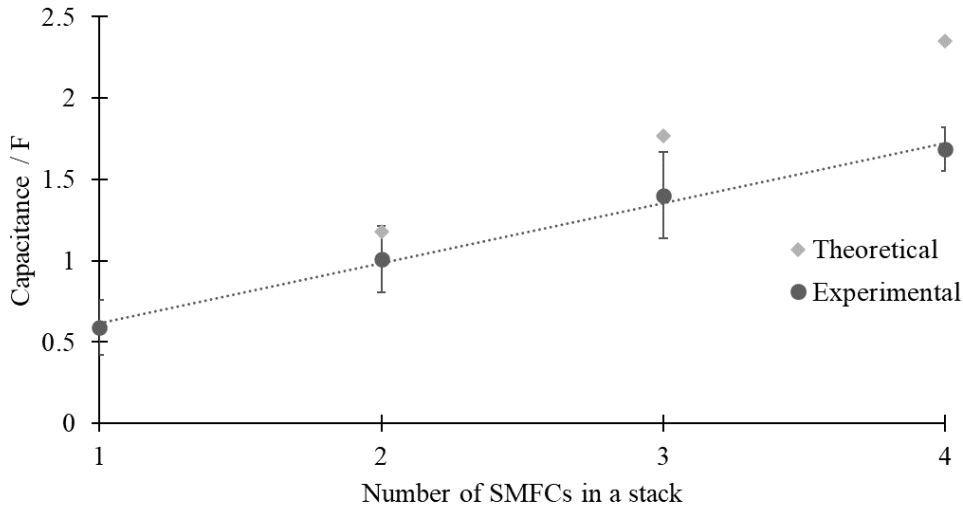
Figure 2S. The behaviour of capacitance when stacking multiple SMFCs in parallel, obtained through open circuit tests. Error bars for a single SMFC and stack of 2, 3 and 4 SMFCs refer to replicates of 8,4, 2 and 2 respectively.
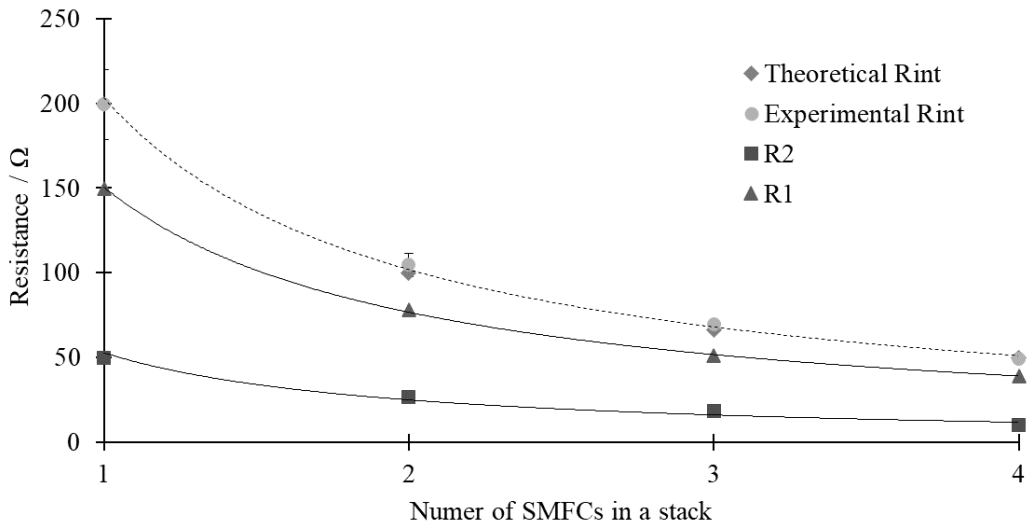

Figure 3S. The behaviour of internal resistance (Rint) when stacking multiple SMFCs in parallel, obtained through polarisation tests and open circuit tests. Error bars for a single SMFC and stack of 2, 3 and 4 SMFCs refer to replicates of 8,4, 2 and 2 respectively
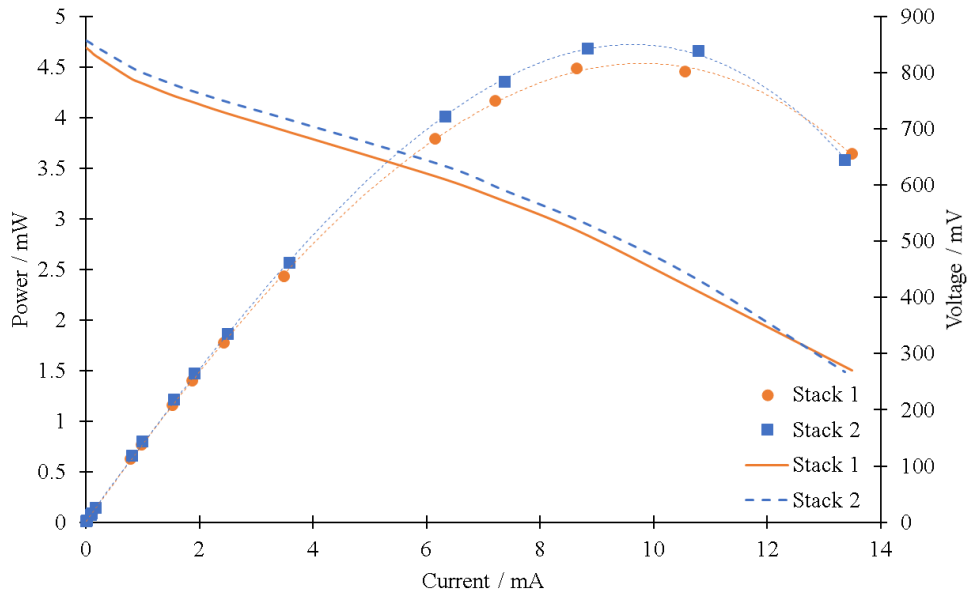
Figure 4S. Power and polarisation curves of the two stacks of 4 SMFCs, generated 2 days prior to connecting the SMFCs to the PMS boxes.